

Journal of Materials Chemistry B

Accepted Manuscript



This is an *Accepted Manuscript*, which has been through the Royal Society of Chemistry peer review process and has been accepted for publication.

Accepted Manuscripts are published online shortly after acceptance, before technical editing, formatting and proof reading. Using this free service, authors can make their results available to the community, in citable form, before we publish the edited article. We will replace this *Accepted Manuscript* with the edited and formatted *Advance Article* as soon as it is available.

You can find more information about *Accepted Manuscripts* in the [Information for Authors](#).

Please note that technical editing may introduce minor changes to the text and/or graphics, which may alter content. The journal's standard [Terms & Conditions](#) and the [Ethical guidelines](#) still apply. In no event shall the Royal Society of Chemistry be held responsible for any errors or omissions in this *Accepted Manuscript* or any consequences arising from the use of any information it contains.

Photodynamic Therapy of Oligoethylene Glycol Dendronized Reduction-Sensitive Porphyrins

Cite this: DOI: 10.1039/x0xx00000x

Lei Xu,^a Lichao Liu,^a Feng Liu,^a Wen Li,^{*b} Ruobin Chen,^b Yun Gao,^a Weian Zhang^{*a}

Received 00th January 2012,
Accepted 00th January 2012

DOI: 10.1039/x0xx00000x

www.rsc.org/

OEGylation of porphyrins via a disulfide linkage to form a novel class of dendritic porphyrin photosensitizers (PSs) is presented. These amphiphilic PSs possess precise molecular structures which could self-assemble into spherical aggregates in aqueous solutions. Their thermoresponsiveness was investigated with UV-Vis spectroscopy, and their reduction responsive properties were inspected with dynamic light scattering and TEM measurements. Moreover, the uptake of porphyrin-containing dendritic micelles by cells and release of reduction-sensitive PSs were investigated with flow cytometry and confocal laser scanning microscopy. The results showed that the cellular uptake of dendritic micelles was more than that of free porphyrin and the uptake process was time-dependent. Additionally, phototoxicity of these dendritic PSs micelles was investigated by MTT assay. It was found that dendritic micelles presented efficient phototoxicity to cancer cells while the free porphyrin had nearly no toxicity under light irradiation. All results indicate that these dendritic PSs are promising for photodynamic therapy.

Introduction

Photodynamic therapy (PDT) is a controllable treatment that involves a photosensitizer, molecules oxygen and light.^{1,2} After irradiation with proper wavelength light, activated photosensitizer generates cytotoxic species which can attack cellular component and lead to the target cells apoptosis or necrosis.³⁻⁷ Compared with traditional therapies of tumors such as chemotherapy, radiation therapy and surgery, PDT shows excellent advantages for its controllable destroying diseased tissue, fast healing process without scarring, fewer side effect and non-invasion.⁸ Thus, PDT has aroused great interests over the past decade for the treatment of neoplasm in skin, bladder, brain, ovarian and so on.^{9,10} So far, some photosensitizers for PDT such as Photofrin, Foscan, Visudyne, Levulan and Metvix have been investigated and obtained clinical approval.¹¹

Up to now, nanostructured carriers including inorganic nanoparticles, micelles and liposomes have been developed for drug delivery systems, since they have been exhibited many

unique features like increasing the solubility of hydrophobic drug in aqueous solutions,¹² prolonging circulating time in blood, selectively accumulating into tumor site by enhancing permeability and retention (EPR) effect and decreasing side effects.¹³⁻¹⁹ Among these nanostructure carriers for drug delivery systems, dendrimers are promising materials since they are characteristics of highly branched, monodispersed, well-defined topological structure, and have large amount of functional peripheral groups.^{13,20-22} Drugs can be loaded on dendrimers via non-covalent interaction or covalent bond with the function groups. Actually, dendrimer-based therapeutics have been widely used in anti-neoplastic agents, bio-imaging, neutron capture therapy, photothermal therapy and photodynamic therapy.²³ For example, Aida *et al.* had exploited an iron (II) porphyrin 1-methylimidazole complex covalently encapsulated within a large aryl ether dendrimer cage, which afforded a long-lived dioxygen adduct.²⁴ Woo-Dong Jang *et al.* had developed a dendritic micelle system for PDT, which consisted of 32 negative charges on the periphery of a third

generation poly (benzyl ether) dendritic zinc porphyrin, and poly (ethylene glycol)-poly (L-lysine) block copolymer in aqueous media.²⁵ Recently, we developed a novel class of oligoethylene glycol (OEG)-based dendrimers which showed attractive thermosensitiveness with tunable phase transition temperatures (LCSTs).^{26,27} These thermo-responsive OEGylated dendrimers were found to be nontoxic and biocompatible, which exhibited a promising application as drug delivery nanocarriers.²⁸

Controlled and enhanced release of drugs at pathological site has been proven to be a great challenge for drug delivery.²⁹ Traditional drug release processes are dependent on the diffusion-controlled, flow-controlled and swelling-controlled processes which have exhibited many drawbacks such as different release rates and limiting selection of drug carriers.³⁰ Much effort has been devoted to the development of stimuli-responsive drug delivery systems which could be responsive to external stimulus including temperature, pH, enzyme, ultrasound, light, oxidation and reduction.³¹⁻³⁷ Disulfide-containing reduction-responsive nanocarriers have been well studied and used in stimuli-responsive drug delivery systems, which can be sensitive to free thiols such as glutathione (GSH).³⁸⁻⁴⁰ An important feature for fabrication of disulfide-containing drug delivery systems is the overexpression of GSH with abundant thiols in cancer cells compared with that in normal cells.⁴¹ The concentration of GSH in intracellular (about 10 mM) is much higher than in extracellular compartment.⁴² Therefore, disulfide-containing nanostructured carriers have received a large amount of interests for intracellular release of the encapsulated drugs.⁴³⁻⁴⁸

Herein, a novel class of disulfide reduction-responsive dendritic amphiphilic drug carriers were constructed for PDT from ethoxyl-terminated first or second generation OEG dendron, Et-Gn (n = 1, 2), with 5-(4-hydroxyphenyl)-10, 15, 20-triphenylporphyrin (TPP-OH). The self-assembly behaviour of these porphyrin disulfide Et-Gn (TPP-S-S-Gn) in aqueous solutions was studied, and their thermo- and reduction-responsive behaviors were investigated by DLS and TEM. Flow cytometry and CLSM were further employed to monitor their location and uptake quantity by checking the fluorescence of porphyrin. Phototoxicity of these porphyrin dendritic micelles was evaluated by MTT assay against MCF-7 cells.

Experimental

Materials

The Et-G1-OH, Et-G2-OH⁴⁹ and 5-(4-hydroxyphenyl)-10, 15, 20-triphenylporphyrin (TPP-OH)⁵⁰ were synthesized according to the previous works, respectively. Dichloromethane (DCM) was dried over CaH₂ and distilled just before use. 1-(3-Dimethylaminopropyl)-3-ethylcarbodiimide hydrochloride (EDC), 4-dimethylaminopyridine (DMAP), 4', 6-diamidino-2-phenylindole (DAPI) and 3-(4, 5-dimethylthiazol-2-yl)-2, 5-diphenyltetrazolium bromide (MTT) were purchased from Aladdin and used as received. Other chemicals were all analytical grade and used as received unless mentioned.

Characterization

The proton NMR spectra were acquired from Bruker 400 MHz NMR spectrometer using CDCl₃ as solvent. UV-Vis spectra were recorded on UV-2450 UV-visible spectrophotometer with a temperature control water bath. Transmittance was monitored at temperature increment of 1 °C with equilibration time of 10 min, and 500 nm was monitored for transmission measurements with a solution concentration of 0.1 mg/mL. The fluorescence spectra were recorded on a F-4500 fluorescence spectrophotometer at room temperature. BECKMAN COULTER Delasa Nano C particle analyzer was used to acquire hydrodynamic diameter at a fixed angle of 165° at room temperature. TEM images were taken on a JEOL JEM1400 electron microscopes operated at 100 kV. TEM samples were prepared by dropping the micelle solution (1 mg/mL) onto a carbon coated copper grid and dried at room temperature.

Synthesis of 6-Porphyrin-1-hexanol (TPPC6-OH).

TPP-OH (0.63 g, 1 mmol), 6-chloro-1-hexanol (0.15 mL, 1.15 mmol) and potassium carbonate (0.14 g, 1 mmol) were mixed in DMF (100 mL). The mixture was refluxed for 12 h and washed with water three times. The product was extracted with DCM, and dried with anhydrous MgSO₄. After the solvent was removed by vacuum evaporation, the crude product was purified on a silica gel column with DCM as eluent. Yield: 0.67 g (91.8 %). ¹H NMR (400 MHz, CDCl₃), δ ppm: 8.87 (m, 8H, β-H), 8.21 (m, 6H, 10,15,20-Ar-*o*-H), 8.11 (m, 2H, 5-Ar-*o*-H), 7.76 (m, 9H, 10,15,20-Ar-*m*- and *p*-H), 7.28 (m, 2H, 5-Ar-*m*-H), 4.26 (t, 2H, -O-CH₂-CH₂-), 3.75 (t, 2H, -CH₂-OH), 2.00 (m, 2H, -O-CH₂-CH₂-CH₂-), 1.76-1.59 (m, 6H, -CH₂-CH₂-CH₂-CH₂-OH), -2.77 (s, 2H, -NH-).

Synthesis of Disulfide-modified Carboxyl Terminal Porphyrin

(TPP-S-S-COOH).

TPP-S-S-COOH was synthesized via esterification by coupling TPPC6-OH with 3, 3'-dithiodipropionic acid. Typically, TPPC6-OH (1.34 g, 2 mmol), 3, 3'-dithiodipropionic acid (0.84 g, 4 mmol) and DMAP (0.246 g, 2 mmol) were dissolved in anhydrous DMF (50 mL) under N₂ atmosphere. After the solution was cooled to 0 °C in an ice-water bath, DCC (0.82 g, 4 mmol) in DMF (5 mL) was added dropwise, and the mixture was stirred at room temperature overnight. Then the mixture was filtered to remove dicyclohexylurea, washed with DCM and brine, and dried with MgSO₄. After removing DCM by evaporation, the crude product was purified on a silica gel column with petroleum ether/ethyl acetate (3:2, v/v) as eluent. Yield: 1.61 g (87.1 %). ¹H NMR (400 MHz, CDCl₃), δ ppm: 8.87 (m, 8H, β-H), 8.21 (m, 6H, 10,15,20-Ar-*o*-H), 8.11 (m, 2H, 5-Ar-*o*-H), 7.76 (m, 9H, 10,15,20-Ar-*m*- and *p*-H), 7.27 (m, 2H, 5-Ar-*m*-H), 4.26 (t, 2H, -O-CH₂-CH₂-), 4.20 (t, 2H, -CH₂-CH₂-O-), 2.96 (m, 4H, -CH₂-CH₂-S- and -S-CH₂-CH₂-), 2.76 (-CO-CH₂-CH₂- and -CH₂-CH₂-CO-) 1.99 (m, 2H, -O-CH₂-CH₂-

CH₂-), 1.84-1.74 (m, 6H, -CH₂-CH₂-CH₂-CH₂-CH₂-O-), -2.77 (s, 2H, -NH-).

Synthesis of Porphyrin Disulfide Coupled Et-Gn (n = 1, 2) (TPP-S-S-Gn).

A representative example for the synthesis of TPP-S-S-Gn is as follows: TPP-S-S-COOH (0.923 g, 1 mmol), Et-G2-OH (2.409 g, 1 mmol), DMAP (0.0061 g, 0.5 mmol) and dry DCM (20 mL) were added into a dry bottle under N₂, and EDC (0.192 g, 1 mmol) in DCM (5 mL) was added drop-wise into the bottle in ice-water bath. After the mixture was stirred at room temperature overnight, the mixture was washed with water, dried with MgSO₄ and filtered. After evaporation of the solvent, the crude product was purified on a silica gel column with petroleum ether/ethyl acetate (1:2 v/v) as eluent. Yield: 2.26 g (67.9 %). ¹H NMR (400 MHz, CDCl₃), δ ppm: 8.87 (m, 8H, β-H), 8.21 (m, 6H, 10,15,20-Ar-*o*-H), 8.11 (m, 2H, 5-Ar-*o*-H), 7.75 (m, 9H, 10,15,20-Ar-*m*- and *p*-H), 7.28 (m, 2H, 5-Ar-*m*-H), 6.64-6.48 (m, 8H, CH), 5.01 (s, 2H, -CO-O-CH₂-CH-), 4.43 (s, 6H, -O-CH₂-CH-), 4.26 (t, 2H, -O-CH₂-CH₂-CH₂-), 4.21 (m, 2H, -CH₂-CH₂-O-), 4.19-4.07 (m, 24H, -CH-O-CH₂-CH₂-), 3.89-3.45 (m, 138H, -O-CH₂-CH₂-O-CH₂-CH₂-O-CH₂-CH₂-O-CH₂-CH₃), 2.95 (t, 4H, -CH₂-CH₂-S- and -S-CH₂-CH₂-), 2.78 (q, 4H, -CO-CH₂-CH₂- and -CH₂-CH₂-CO-), 2.00 (m, 2H, -O-CH₂-CH₂-CH₂-), 1.84-1.64 (m, 6H, -O-CH₂-CH₂-CH₂-CH₂-CH₂-CH₂-O-), 1.20 (t, 27H, -CH₂-CH₃), -2.77 (s, 2H, -NH-). MALDI-TOF-MS spectrum for TPP-S-S-G2, calcd for C₁₇₄H₂₅₄N₄O₅₃S₂, 3 314.04; found 3 312.51 (Fig. S5).

Self-assembly of TPP-S-S-Gn in aqueous solution.

TPP-S-S-Gn in THF (0.5 mL, 2 mg/mL) was added dropwise into water and then gradually dialyzed against water using a dialysis membrane (MWCO = 12 000) to remove THF. The dialysis was repeated at least three times to make sure THF was removed completely.

Pyrene was used as a fluorescence probe to determine the critical micelle concentration (CMC). The concentration of TPP-S-S-Gn was varied from 0.0002 mg/mL to 0.01 mg/mL, while the concentration of pyrene was fixed at 1 μM. The fluorescence spectra were recorded using F-4500 fluorescence spectrometer with the excitation wavelength of 335 nm. The emission fluorescence at 372 and 383 nm were monitored for the calculation of critical micelle concentration.

Fluorescence Quantum Yields

Fluorescence quantum yield (Φ_u) of TPP-S-S-Gn micelles were measured by a comparative method using H₂TPP as a standard using the Eq. (1)^{51,52}

$$\Phi_u = \Phi_s \frac{A_u I_s \lambda_s n_u^2}{A_s I_u \lambda_u n_s^2} \quad (1)$$

Where, Φ is fluorescence quantum yield; I is absorbance; A is integrated fluorescence intensity; λ is excitation wavelength and n is refractive index of solution. The subscript “s” and “u” represent the standard and the sample, respectively.

Singlet Oxygen Quantum Yields

Singlet oxygen quantum yield (Φ_Δ) was carried out according to the previous literature⁵³⁻⁵⁵. 1, 3-Diphenylisobenzofuran (DPBF) was used as a scavenger to determine the Φ_Δ . The quantum yield of ¹O₂ generation by TPP-S-S-Gn was determined by comparing with H₂TPP as a standard, which has a quantum yield of 0.62 in CCl₄. The DPBF decay at 410 nm was monitored every 10 s. The singlet oxygen quantum was calculated according to Eq. (2):

$$\Phi_\Delta = \Phi_\Delta^{\text{Std}} \frac{R I_{\text{abs}}^{\text{Std}}}{R^{\text{Std}} I_{\text{abs}}} \quad (2)$$

Where, Φ_Δ^{Std} is the singlet oxygen quantum yields for the standard H₂TPP ($\Phi_\Delta^{\text{Std}} = 0.62$ in CCl₄); R and R^{Std} are the DPBF photobleaching rates in the presence of the analyte and the standard, respectively; I_{abs} and $I_{\text{abs}}^{\text{Std}}$ are the rates of light absorption by the analyte and the standard, respectively. The concentration of the quencher (DPBF) was lowered than 3×10^{-5} M to avoid chain reactions induced by quenchers (DPBF) in the presence of singlet oxygen. The experiments were carried out in CCl₄.

Reduction-destabilization of TPP-S-S-Gn Micelles.

TPP-S-S-Gn micelles aqueous solution (1 mg/mL) were mixed with dithiothreitol (DTT) (10 mM) in PBS (pH = 7.4) solution, and then the mixed solvent was placed in a shaking bed at 37 °C with a rotation speed of 100 rpm. The size of the micelles was checked by DLS measurement at different times (4 h and 24 h).

Reduction-release of Porphyrin from TPP-S-S-Gn Micelles.

The release profiles of porphyrin from TPP-S-S-Gn were studied using a membrane tubing (MWCO = 12 000) and immersed in a glass bottle containing PBS (pH = 7.4, 20 mL) or PBS with DTT (10 mM) in a shaking bed at 37 °C. At desired time intervals, 1 mL of external buffer solution was taken out and replenished with an equal volume of fresh media. The amount of released porphyrin was determined by using HPLC with C18 Eclipse-XDB column (250 mm × 4.6 mm). The mobile phase was pure acetonitrile, and the flow rate was maintained at 1.0 mL/min and detection wavelength was 420 nm. The release experiments were carried out in triplicate. Before this analysis, the standard curve of porphyrin was calibrated by HPLC. The control experiment was also carried out without DDT.

Cell Culture

MCF-7 (human breast adenocarcinoma line) were cultivated in DMEM (Dulbecco's modified Eagle's medium) containing 10% FBS (fetal bovine serum) and 1% antibiotics (50 units/mL penicillin and 50 units/mL streptomycin) at 37 °C in a humidified atmosphere containing 5% CO₂. Cells were then treated with the medium containing various micelles or free porphyrin at different doses.

Intracellular Uptake

MCF-7 cells were seeded on sterile cover glasses in a 6-well plate at a density of 1×10^5 cells/well and incubated overnight. Then the culture medium was replaced by fresh medium containing free porphyrin or TPP-S-S-Gn micelles and incubated for 4 h and 24 h, respectively. Cells were fixed with 4% paraformaldehyde in PBS (pH = 7.4) for 30 min and washed 3 times with PBS, and then stained with 4', 6-diamidino-2-phenylindole (DAPI) to mark the nuclei. The cover glasses were placed onto slides for confocal laser scanning microscopy (CLSM) observation which was performed by a fluorescence microscope (Nikon AIR).

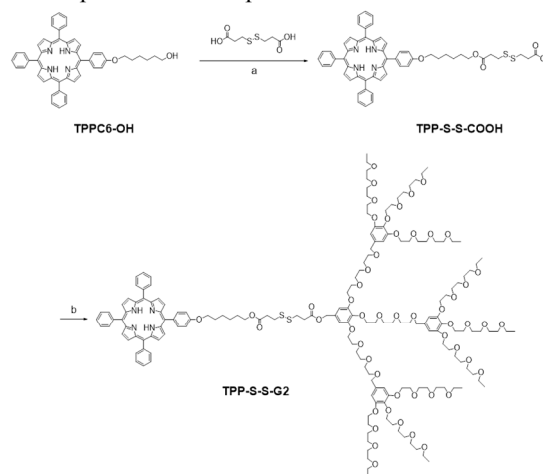
Fluorescence-activated cell sorting (FACS) was also employed to monitor the cellular uptake of free porphyrin and TPP-S-S-Gn micelles, respectively. MCF-7 cells were seeded in a 6-well plate at the density of 1×10^6 cells/well and incubated for 4 h and 24 h, respectively. After predetermined time, the cells were washed, harvested and resuspended with PBS and then monitored with fluorescence-activated cell sorting by using a FACScan flow cytometer (BD LSRFortessa). 10 000 Cells were counted for each sample and the fluorescence of porphyrin was checked.

In Vitro Dark Cytotoxicity and Phototoxicity of TPP-S-S-Gn

Micelles

The cell suspension (200 μL) of MCF-7 with density of 7 000 cells/well were seeded into a 96-well plate. After incubated for 24 h, the MCF-7 cells were treated with different dose of free porphyrin and P-S-S-Gn micelles in FBS-free DMEM at 37 °C for 24 h, and then the media were replaced with fresh DMEM culture medium. The cells were irradiated by a light emitting diodes (LEDs) lamp (400 mW/cm²) for 20 min and then were incubated for 24 h. 20 μL of 3-(4, 5-dimethylthiazol-2-yl)-2, 5-diphenyltetrazolium bromide (MTT) solution (5 mg/mL) was added to each well for a further incubation of 4 h, followed by replacement with 150 μL DMSO to extract the formazan products with gentle agitation for 10 min. The absorbance at 560 nm was detected with spectrophotometric microplate reader (SpectraMax). The cell viability was calculated as follows: cell viability (%) = $(OD_{\text{test}} - OD_{\text{back ground}}) / (OD_{\text{control}} - OD_{\text{back ground}}) \times 100$, where OD_{test} and OD_{control} were respectively the absorbance of the presence of sample solutions and that without treatment. The in vitro dark cytotoxicity of TPP-S-S-Gn or free porphyrin was checked as the same procedure with the phototoxicity of TPP-S-S-Gn described above but without illumination.

To observe the PDT efficiency directly, MCF-7 cells were also stained with calcein-AM and PI after irradiation. MCF-7 cells were seeded onto a 6-well plate with 2×10^5 cells per well and incubated for 24 h. Then the medium was replaced by fresh medium containing 100 μg/mL porphyrin or fresh medium without micelles as a control. After incubation for another 24 h in dark, the cells were irradiated with light for 20 min. After irradiation, the cells were further incubated for 24 h, and then washed with PBS and stained with calcein-AM and PI. All the cell experiment was repeated for three times.



Scheme 1. Synthesis of the TPP-S-S-G2. (a) DCC/DMAP, R.T., 24 h; (b) Et-G2-OH, EDC/DMAP, R.T., 24 h.

Results and Discussion

Synthesis of Porphyrin Disulfide Coupled Gn-Et (n = 1, 2) (TPP-S-S-Gn)

The synthesis routes for TPP-S-S-G2 were shown in **Scheme 1**. TPPC6-OH was firstly prepared from TPP-OH by etherification with 6-chloro-1-hexanol in DMF at 100 °C for 12 h. The ¹H NMR of TPPC6-OH was shown in **Fig. S1**. The proton signals at $\delta = 4.26, 3.75$ and 2.0 are attributed to the methylene protons from $-O-CH_2-CH_2-$, $-CH_2-OH$ and $-O-CH_2-CH_2-CH_2-$ of TPPC6-OH moiety, respectively. The hydroxyl group of TPPC6-OH was then changed to carboxyl group by esterification with 3, 3'-dithiodipropionic acid at room temperature. Here, disulfide bond was introduced in this system which is reduction-sensitive to GSH. After esterification reaction, the methylene proton signal at 3.75 ppm (peak h in **Fig. S1**) shifts to 4.20 ppm (peak g in **Fig. S2**), and two new signals appear at 2.96 and 2.76 ppm, which are ascribed to methylene protons adjacent to disulphide and carbonyl groups.

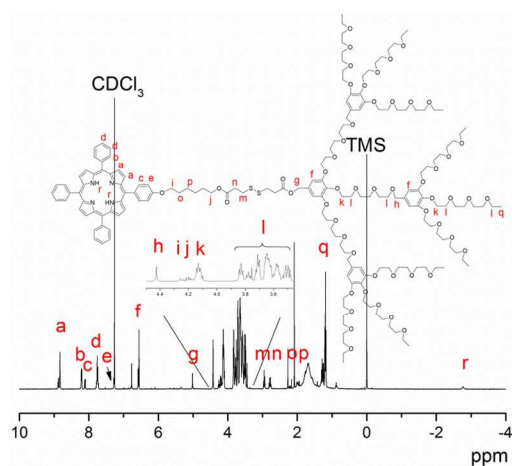


Fig. 1. $^1\text{H-NMR}$ spectrum of TPP-S-S-G2 in CDCl_3 .

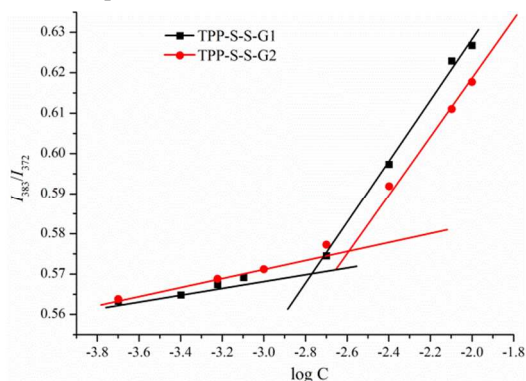


Fig. 2. Fluorescence intensity ratio I_{383}/I_{372} of pyrene as a function of logarithm of TPP-S-S-Gn concentration.

The three-folded oligoethylene glycol-based dendrons Et-G1-OH and Et-G2-OH exhibited attractive properties such as amphiphilicity, biocompatibility and thermoresponsiveness. TPP-S-S-COOH was attached to these dendrons through esterification reaction in the presence of EDC/DMAP. The ^1H NMR spectrum of TPP-S-S-G2 was shown in **Fig. 1**. The proton signals at $\delta = 3.89\text{--}3.45$ and 1.2 ppm are ascribed to the methylene groups and the terminal methyl groups of OEG, respectively, and the proton signals at $\delta = 5.01$ and 4.43 ppm belong to benzyl of the OEG dendron moiety. The proton signals at $\delta = 8.87, 8.21, 8.11, 7.75, 7.28$ and -2.77 ppm are all attributed to porphyrin ring. Moreover, the integral area ratio of imino group (peak a) with methyl group (peak q) is almost equal to the theoretical value (1:9). Thus, ^1H NMR results clearly confirmed successful synthesis of TPP-S-S-G2. The TPP-S-S-G1 was also successfully prepared and its structure confirmed by ^1H NMR spectrum (**Fig. S3**).

Formation and Reduction-Responsive Disruption of TPP-S-S-Gn Micelle in Water

Micelles were prepared by adding TPP-S-S-Gn/THF solution drop-wise into water and then dialyzed against water to remove THF. The critical micelle concentration (CMC) was determined by using pyrene as fluorescence probe. In aqueous solution,

pyrene can transfer into hydrophobic interior of micelles and result in significant spectroscopic changes. The ratio of pyrene fluorescence intensities excited at 383 and 372 nm (I_{383}/I_{372}) was plotted as a function of the logarithm of the concentration of TPP-S-S-Gn micelles. As shown in **Fig. 2**, the ratio of I_{383}/I_{372} increases slowly in low concentration but with a sharp increase after the concentration reached a certain value, which indicates the formation of micelles. Finally, the CMC value of TPP-S-S-G1 and P-S-S-G2 was 1.71×10^{-3} mg/mL and 2.57×10^{-3} mg/mL, respectively. P-S-S-G2 has a higher CMC, since it has a larger hydrophilic segment of OEG.

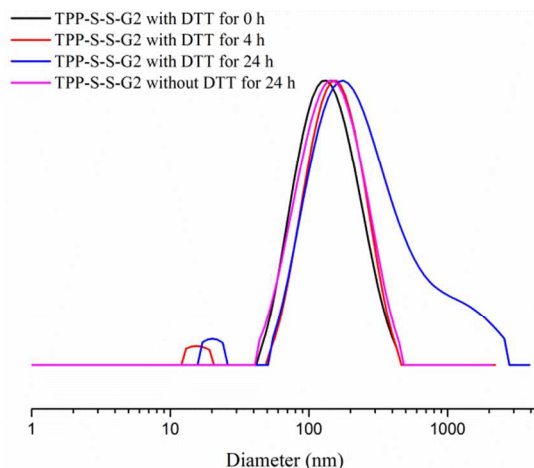


Fig. 3. Size distribution of TPP-S-S-G2 micelles determined by DLS. Blank line: DTT for 0 h, red line: DTT for 4 h, green line: DTT for 24 h, pink line: without DTT for 24 h.

TEM and DLS were employed to study reduction property of TPP-S-S-Gn micelles in response to 10 mM DTT. TEM images (**Fig. 4a** and **4d**) show that the TPP-S-S-G1 and TPP-S-S-G2 all could form spherical aggregates in water. Moreover, the size of TPP-S-S-G2 micelles is slightly bigger than that of TPP-S-S-G1 micelles, which could be resulted from the structures of the G2 dendrons. TPP-S-S-G2 has long OEG chains, leading to a bigger corona. In this system, reduction-responsive disulfide bond was introduced into dendritic molecules, which could be broken by GSH in cancer cells. It is well-known that DTT could oxidize the disulfide bond of dendrimer and disrupt the micelles. After treating with DTT, the spherical micelles were destroyed and some aggregates were formed at 4 h and 24 h. As seen in **Fig. 4b, 4c, 4e** and **4f**, the spherical aggregates of TPP-S-S-Gn were disrupted by DTT to form larger aggregates. DLS was also used to characterize these micelles, and the results showed that the diameter of TPP-S-S-G1 micelles was 116.4 nm with $\text{PDI} = 0.166$ and that of TPP-S-S-G2 was 126.6 with $\text{PDI} = 0.227$. After TPP-S-S-Gn micelles were treated with DTT for 4 h, the main scattering peak shifts to a higher diameter, accompanying appearance of a new small peak in the lower diameter range (**Fig. 3**). Moreover, when treated by DTT for 24 h, there is not only a small peak in the range of lower diameter, but also the main scattering peak becomes much broader, and a big shoulder appears in the peak, suggesting the micelles disrupted by DTT. A similar result was also observed

for TPP-S-S-G1 micelles (Fig. S6). For comparison, the stability of TPP-S-S-Gn micelles after 24 h in the absence of DTT under the same conditions was also studied with DLS, and the results showed the diameter and PDI of TPP-S-S-Gn micelles had nearly no change.

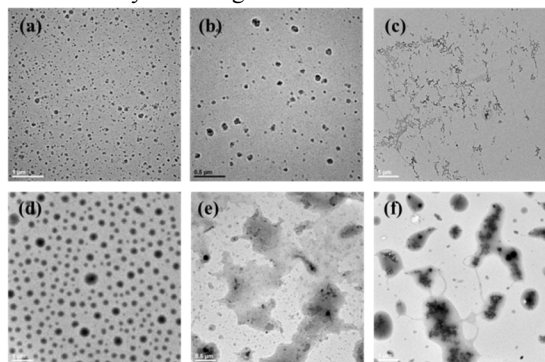


Fig. 4. TEM images of TPP-S-S-G1 (a, b, c) and TPP-S-S-G2 micelles (d, e, f) with treatment using DDT at different time; (a) (d) DTT for 0 h (scale bar, 1 μm), (b) (e) DTT for 4 h (scale bar, 0.5 μm), (c) (f) DTT for 24 h (scale bar, 1 μm).

The stability and zeta potential of TPP-S-S-Gn micelles in PBS and DMEM at 37 $^{\circ}\text{C}$ were further evaluated, respectively. As shown in Fig. S7 and Table S1, the two kinds of micelles were all quite stable in PBS for 10 days besides the PDI of TPP-S-S-G2 micelles became broad. For the TPP-S-S-Gn micelles in DMEM, it can be seen that the smaller peaks appeared at the lower diameter range, but the main peaks are very similar with that of micelles in water or PBS. The appearance of small peaks should be resulted for the formation of the small particles. After 10 days, TPP-S-S-G1 micelles in DMEM were also quite stable except for some change of the small aggregates. However, for TPP-S-S-G2 micelles in DMEM, the PDI obviously became broad, although the size of the aggregates did not increase after 10 days. Additionally, the zeta potential of TPP-S-S-G1 and TPP-S-S-G2 micelles in PBS was -34.42 mV and -29.34 mV, and then changed to -13.26 mV and -16.81 mV after 10 days, separately. The decrease of the zeta potential of TPP-S-S-Gn micelles was also found in DMEM, which further confirms the DLS results.

Thermoresponsive Behavior

The thermoresponsiveness of these two dendritic TPP-S-S-Gn was respectively evaluated in aqueous solutions by checking the transmittance at 550 nm. As shown in Fig. 5, both TPP-S-S-G1 and TPP-S-S-G2 are thermoresponsive and showing abrupt phase transitions with their LCSTs at 32.4 $^{\circ}\text{C}$ and 35.8 $^{\circ}\text{C}$, respectively. Their LCSTs were dependent on the mass ratio of the hydrophilic OEG dendrons to hydrophobic porphyrin. The TPP-S-S-G2 contains more OEG units than TPP-S-S-G1, which means TPP-S-S-G2 is more hydrophilic, resulting in a higher LCST. Below LCST, OEG chains were surrounded with water molecules to ensure their water solubility. When the temperature was above LCST, the bounded water molecules escaped from OEG chains and these chains tended to shrink.⁵⁶ The entropy gain in the process of bounded water released from

TPP-S-S-G2 was higher than that of TPP-S-S-G1 which compensated by temperature.⁵⁷ So the LCST of TPP-S-S-Gn was mainly dependent on the mass ratio of the hydrophilic OEG dendrons to hydrophobic porphyrin.

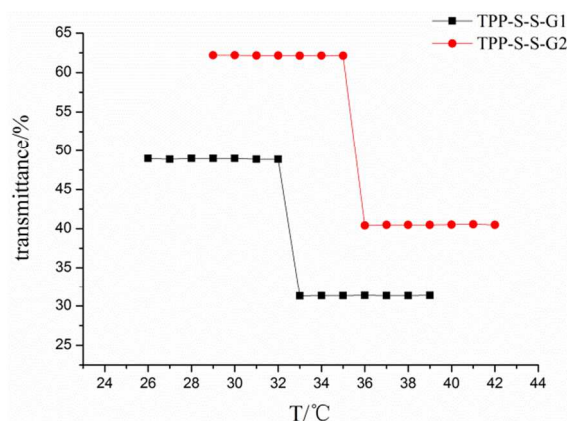


Fig. 5. Temperature dependences of transmittance at 550 nm obtained for aqueous solutions of TPP-S-S-G1 (0.1 mg/mL) and TPP-S-S-G2 (0.1 mg/mL).

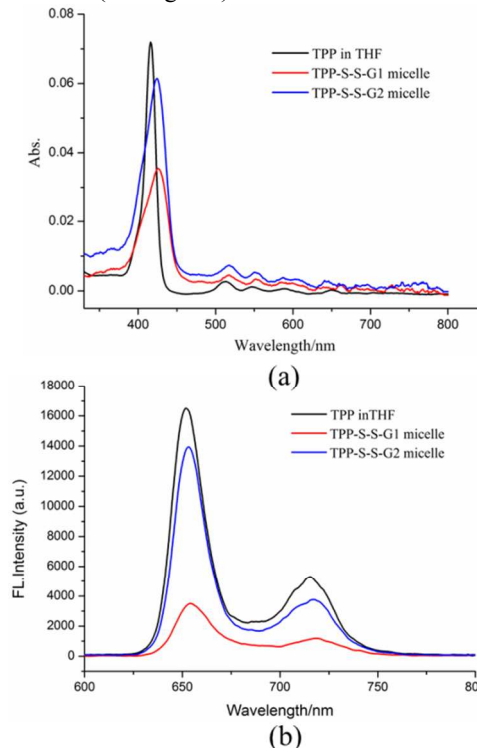


Fig. 6. (a) UV-Vis absorption spectra of TPP-S-S-Gn micelles in pure water, and (b) fluorescence emission spectra of TPP-S-S-Gn micelles.

Fluorescence Quantum Yields and Singlet Oxygen Quantum Yields

The fluorescence quantum yield of these two TPP-S-S-Gn dendritic micelles in water were checked by UV and

fluorescence spectrophotometer by using TPP as standard, and the results were shown in **Fig. 6**. According to eq. (1), the fluorescence quantum yields of TPP-S-S-G1 and TPP-S-S-G2 were 0.011 and 0.028, separately, which were 5-10 fold lower than that of the control H_2TPP (0.11). Additionally, the UV-vis spectra (**Fig. 6a**) of TPP-S-S-G1 and TPP-S-S-G2 micelles showed that the micelles had a clear red shift compared to H_2TPP/THF solution. The red shift indicates that the porphyrin moieties were π -stacking with each other in micelle core, which causes the decrease of the fluorescence quantum yield.

The singlet oxygen quantum yields of TPP-S-S-Gn were also measured. After irradiation, the energy transfer from excited triplet state of porphyrin to ground state of oxygen to generate singlet oxygen. DPBF was used to capture singlet oxygen, and the peak intensity of the mixture of DPBF and TPP-S-S-Gn in CCl_4 was checked by using UV-Vis spectrophotometer (**Fig. 7**). The singlet oxygen quantum yield of TPP-S-S-G1 and TPP-S-S-G2 was 0.614 and 0.623, respectively, which was calculated according to Eq. (2). Thus, these two dendritic porphyrin derivatives had a similar singlet oxygen quantum compared to H_2TPP (0.62).

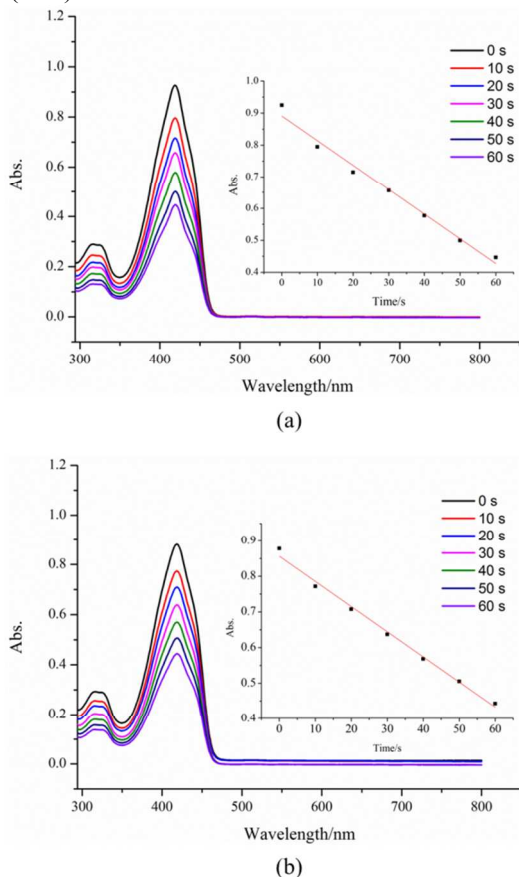


Fig. 7 UV-Vis absorption spectra of DPBF with (a) TPP-S-S-G1 and (b) TPP-S-S-G2 after irradiation for different times in CCl_4 (inset: plot of absorbance versus time).

Reduction-Release of Porphyrin from TPP-S-S-Gn Micelles

In vitro release of porphyrin from TPP-S-S-Gn micelles were investigated by using dialysis tube (MWCO = 12 000) in PBS buffer (pH = 7.4) at 37 °C with gentle shaking in the presence or absence of 10 mM DTT. As shown in **Fig. 8**, TPP-S-S-G1 and TPP-S-S-G2 micelles have a similar release behavior of porphyrin at the same conditions. At the first 20 h, the porphyrin had a rapid release rate, and about 60% porphyrins were released under the treatment of 10 mM DTT. In contrast, there is nearly no porphyrin released from the TPP-S-S-Gn micelles without treatment of DTT. Thus, the result of vitro drug release clearly demonstrated that these micelles were reduction-responsive, which could effectively release porphyrin moieties in response to GSH inside the cells.

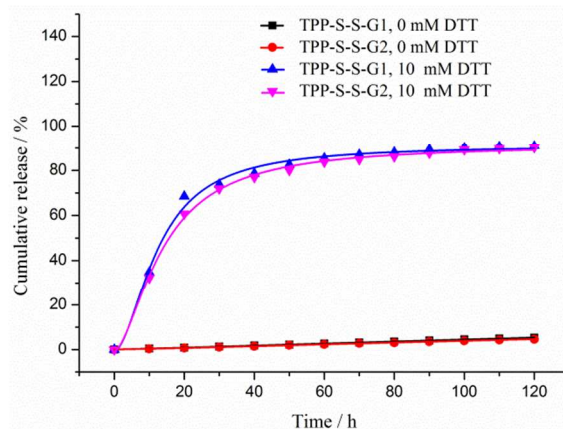


Fig. 8 The reduction behavior of porphyrin released from TPP-S-S-G1 and TPP-S-S-G2 micelles with and without the treatment of DTT. The profiles of porphyrin were recorded at 37 °C with pH = 7.4.

In vitro cellular uptake of TPP-S-S-Gn Micelles

The cellular uptake and intracellular distribution of free porphyrin and TPP-S-S-Gn micelles in vitro were evaluated using MCF-7 by flow cytometry and confocal laser scanning microscopy, respectively (**Scheme 2**). For quantitative determination of the fluorescence of porphyrin inside cells, the TPP-S-S-Gn micelles were added to culture medium with porphyrin concentration of 50 $\mu g/mL$ and cells were incubated for 4 h and 24 h. As shown in **Fig. 9**, after 4 h incubation with free porphyrin and TPP-S-S-G2 micelles, we could clearly see that the fluorescence intensity of TPP-S-S-G2 micelles were higher than that of control, indicating the cells had taken in porphyrin and TPP-S-S-G2 micelles. Moreover, the fluorescence peak of TPP-S-S-G2 micelles shifts to the right compared to that of free porphyrin with the same incubation time, which means more TPP-S-S-G2 micelles had been taken than free porphyrin. With increasing the incubation time for 24 h, the fluorescence intensity increases whenever for free porphyrin and TPP-S-S-G2 micelles, which could be attributed to persistent uptake of these photosensitive agents. It is well known that free porphyrin was transported to cells via passive diffusion mechanism, but the TPP-S-S-G2 micelles may be internalized by an endocytosis process.^{58,59}

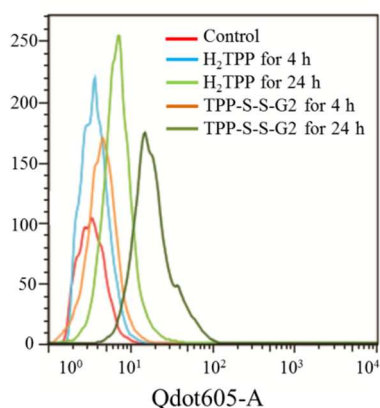


Fig. 9. The cellular uptake of free porphyrin and TPP-S-S-G2 micelles at different time, red line: control, blue line: free porphyrin for 4h, aqua line: free porphyrin for 24 h, orange line: TPP-S-S-G2 for 4 h, black green line: TPP-S-S-G2 for 24 h.

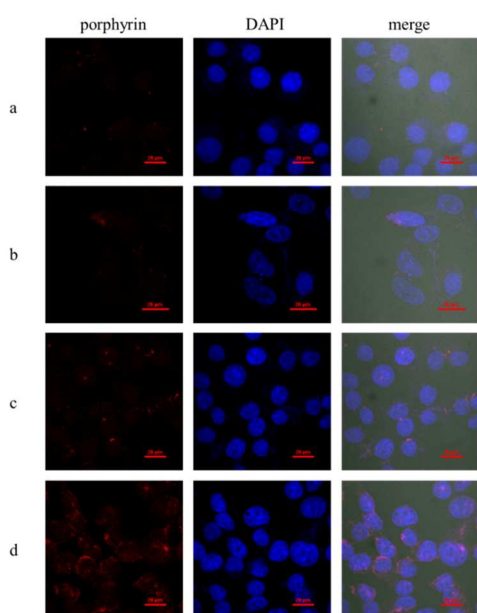


Fig. 10. Confocal laser scanning microscopy images of cellular internalization of free porphyrin and TPP-S-S-G2 micelles with MCF-7 cells (a) free porphyrin for 4 h, (b) free porphyrin for 24 h, (c) TPP-S-S-G2 for 4 h, (d) TPP-S-S-G2 for 24 h. The images from left to right were porphyrin fluorescence, nuclear staining with DAPI and overlays of images. Scale bar: 20 μm .

Confocal laser scanning microscopy was further employed to investigate cellular uptake of free porphyrin and TPP-S-S-Gn micelles. MCF-7 cells were cultured with free porphyrin and TPP-S-S-Gn micelles with porphyrin concentration of 50 $\mu\text{g}/\text{mL}$ for 4 h and 24 h, respectively. DAPI was used to stain nucleus after the predetermined interval time. From CLSM results in **Fig. 10**, weak fluorescence intensity of free porphyrin and TPP-S-S-G2 micelles were obtained after incubation for 4 h, but the intensities obviously became stronger after incubation for 24 h. Meanwhile, we also found that the fluorescence of TPP-S-S-G2 was also stronger than that of free porphyrin for

either 4 h or 24 h. The result indicated that the micelles might be uptaken by a time-dependent process which is agreement with the results of flow cytometry mentioned above.

The cellular uptake and intracellular distribution of TPP-S-S-G1 micelles were also evaluated. We obtained the similar result to TPP-S-S-G2, where the fluorescence of TPP-S-S-G1 shift right compared to that of free porphyrin at the same incubation time (**Fig. S9**), and the fluorescence intensity also stronger than that of free porphyrin (**Fig. S10**). However, when comparing the flow cytometry between the two generations, the geometrical mean fluorescence of TPP-S-S-G2 was higher than that of TPP-S-S-G1. This may be because second generation TPP-S-S-G2 carry more OEG moieties outside as the coronal which could help cells endocytosis.

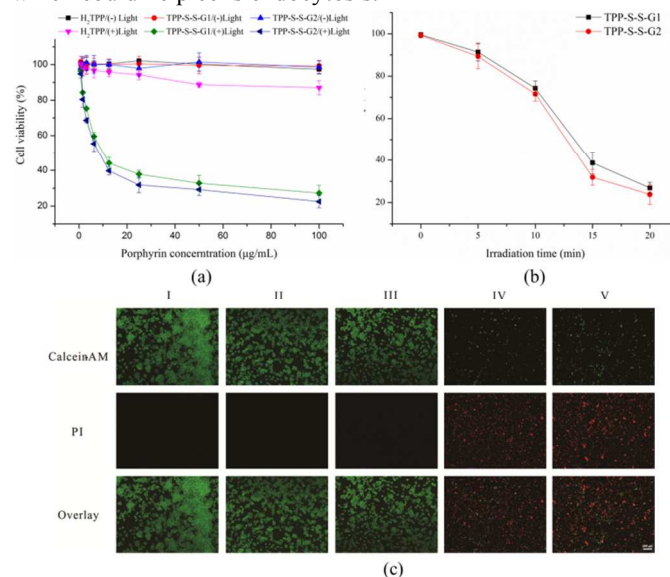
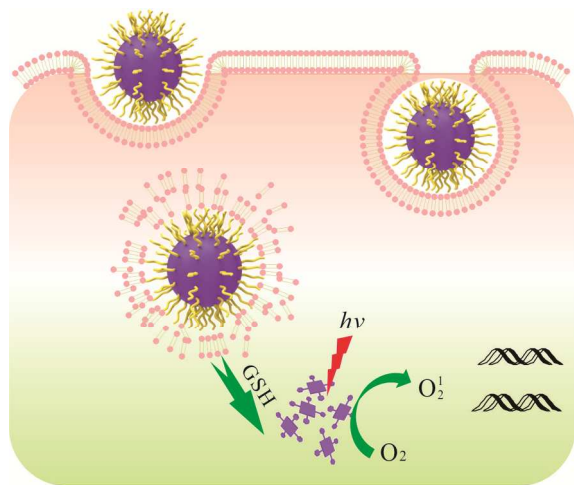


Fig. 11. In vitro cytotoxicity of TPP-S-S-Gn micelles against MCF-7 cells: (a) dark cytotoxicity and phototoxicity of different porphyrin concentration, (b) the phototoxicity of TPP-S-S-Gn under different irradiation time, (c) double-staining with calcein AM and PI to detect the PDT efficacy, dead cells: red fluorescence of PI and live cells: green fluorescence of calcein AM, I: control, II: TPP-S-S-G1/light(-), III: TPP-S-S-G2/light(-), IV: TPP-S-S-G1/light(+), V: TPP-S-S-G2/light(+), porphyrin concentration was 100 $\mu\text{g}/\text{mL}$, scale bar: 200 μm , n=3.

Dark Cytotoxicity and Phototoxicity of TPP-S-S-Gn Micelles.

To estimate the PDT efficiency of TPP-S-S-Gn micelles, we performed in vitro phototoxicity with or without light treatment on MCF-7 cells. MTT was used to determine cell viability, and the cells in dark without treatment were set to the viability of 100% as reference. We first studied the dark cytotoxicity of free porphyrin and TPP-S-S-Gn micelles. As shown in **Fig. 11a**, no obvious dark cytotoxicity against MCF-7 cells was observed even the porphyrin concentration at 100 $\mu\text{g}/\text{mL}$. Then the phototoxicity was studied by irradiation with visible light LED lamps (400 mW/cm^2) for 20 min. For free porphyrin, there was no significant difference between its dark cytotoxicity and

phototoxicity, which may be because free porphyrin had low internalization efficiency. However, we found that the phototoxicity of TPP-S-S-Gn micelles was much higher than that of free porphyrin with the IC₅₀ (calculated for porphyrin concentration) of 9.95 µg/mL (TPP-S-S-G1) and 8.24 µg/mL (TPP-S-S-G2), respectively. Actually, the cell viability of these two TPP-S-S-Gn at the porphyrin concentration of 100 µg/mL was 27.2% and 22.5%, separately. Additionally, these two TPP-S-S-Gn dendrimers had the nearly same phototoxicity, but they were much higher than free porphyrin. We also evaluated the phototoxicity of TPP-S-S-Gn micelles with different irradiation time varied from 5, 10, 15 to 20 min at the porphyrin concentration of 100 µg/mL. As shown in Fig. 11b, the cell viability of cancer cells clearly decreased with increasing irradiation time whenever for TPP-S-S-G1 or TPP-S-S-G2 micelles. The calcein-AM and PI were further employed to stain the cells for direct observation of the PDT efficiency (Fig. 11c). Live and dead cells present as green and red fluorescence using these two dyes, respectively. After MCF-7 cells were treated with TPP-S-S-Gn micelles for 24 h, there was no red fluorescence detected, indicating TPP-S-S-Gn micelles had no cytotoxicity for these cells. However, above MCF-7 cells treated with TPP-S-S-Gn micelles were irradiated with light for 20 min, and then the remarkable red fluorescence appeared in Fig. 11c, which means that the cells were killed by TPP-S-S-Gn micelles under light irradiation. Thus, the result shows TPP-S-S-Gn dendrimers will have the potential applications for PDT.



Scheme 2. Illustration of TPP-S-S-Gn micelles for intracellular PDT.

Conclusion

First and second generation of monodisperse amphiphilic dendritic porphyrins TPP-S-S-G1 and TPP-S-S-G2 were efficiently synthesized via esterification from porphyrin disulfide and Et-Gn-OH. Both dendritic porphyrins could self-assemble into spherical micelles in water, and exhibit excellent thermoresponsive behavior with LCST between 32.4 °C and 35.8 °C. The disulfide bond in TPP-S-S-Gn affords them

reduction-sensitivity, and their *in vitro* release of reduction-sensitive PSs could be well controlled by DTT. Flow cytometry and CLSM results showed that the cellular uptake of TPP-S-S-Gn micelles was more than that of free porphyrin and the uptake process was time-dependent. From MTT assay, TPP-S-S-Gn micelles presented efficient phototoxicity to MCF-7 cells while the free porphyrin showed nearly no toxicity under light irradiation. Therefore, these porphyrin-containing reduction-sensitive dendritic photosensitizers are promising for the photodynamic therapy.

Acknowledgements

This work was financially supported by the National Natural Science Foundation of China (No.51173044), Research Innovation Program of SMEC (No.14ZZ065), and Shanghai Pujiang Program under 14PJ1402600. W. Z. also acknowledges the support from the Fundamental Research Funds for the Central Universities.

Notes and references

^a Shanghai Key Laboratory of Functional Materials Chemistry, School of Materials Science and Engineering, East China University of Science and Technology, 130 Meilong Road, Shanghai 200237, P. R. China

^b Laboratory of Polymer Chemistry, Department of Polymer Materials, College of Materials Science and Engineering, Shanghai University, Nanchen Street 333, Materials Building Room 433, Shanghai 200444, China

*Correspondence to: Weian Zhang (E-mail: wazhang@ecust.edu.cn)

Wen Li (E-mail: wli@shu.edu.cn)

† Electronic Supplementary Information (ESI) available: Experimental details and characterization data. See DOI: 10.1039/c000000x/

(1) Dougherty, T. J.; Gomer, C. J.; Henderson, B. W.; Jori, G.; Kessel, D.; Korblik, M.; Moan, J.; Peng, Q. *Journal of the National Cancer Institute* **1998**, *90*, 889.

(2) Ethirajan, M.; Chen, Y.; Joshi, P.; Pandey, R. K. *Chemical Society Reviews* **2011**, *40*, 340.

- (3) Agostinis, P.; Berg, K.; Cengel, K. A.; Foster, T. H.; Girotti, A. W.; Gollnick, S. O.; Hahn, S. M.; Hamblin, M. R.; Juzeniene, A.; Kessel, D.; Korbek, M.; Moan, J.; Mroz, P.; Nowis, D.; Piette, J.; Wilson, B. C.; Golab, J. *CA: A Cancer Journal for Clinicians* **2011**, *61*, 250.
- (4) Hsu, C. Y.; Nieh, M. P.; Lai, P. S. *Chemical Communications* **2012**, *48*, 9343.
- (5) Lee, C.-S.; Na, K. *Biomacromolecules* **2014**.
- (6) Nakamura, H.; Liao, L.; Hitaka, Y.; Tsukigawa, K.; Subr, V.; Fang, J.; Ulbrich, K.; Maeda, H. *Journal of Controlled Release* **2013**, *165*, 191.
- (7) Wang, C.; Sun, X. Q.; Cheng, L.; Yin, S. N.; Yang, G. B.; Li, Y. G.; Liu, Z. *Advanced Materials* **2014**, *26*, 4794.
- (8) Lovell, J. F.; Liu, T. W. B.; Chen, J.; Zheng, G. *Chemical Reviews* **2010**, *110*, 2839.
- (9) Dolmans, D. E. J. G. J.; Fukumura, D.; Jain, R. K. *Nat Rev Cancer* **2003**, *3*, 380.
- (10) Triesscheijn, M.; Baas, P.; Schellens, J. H. M.; Stewart, F. A. *The Oncologist* **2006**, *11*, 1034.
- (11) Voon, S. H.; Kiew, L. V.; Lee, H. B.; Lim, S. H.; Noordin, M. I.; Kamkaew, A.; Burgess, K.; Chung, L. Y. *Small* **2014**, n/a.
- (12) Ornelas, C.; Mery, D.; Cloutet, E.; Aranzaes, J. R.; Astruc, D. *Journal of the American Chemical Society* **2008**, *130*, 1495.
- (13) Mintzer, M. A.; Grinstaff, M. W. *Chemical Society Reviews* **2011**, *40*, 173.
- (14) Elsabahy, M.; Wooley, K. L. *Chemical Society Reviews* **2012**, *41*, 2545.
- (15) Li, L.; Huh, K. M.; Lee, Y.-K.; Kim, S. Y. *Journal of Materials Chemistry* **2011**, *21*, 15288.
- (16) Nicolas, J.; Mura, S.; Brambilla, D.; Mackiewicz, N.; Couvreur, P. *Chemical Society Reviews* **2013**, *42*, 1147.
- (17) Singh, A.; Talekar, M.; Tran, T.-H.; Samanta, A.; Sundaram, R.; Amiji, M. *Journal of Materials Chemistry B* **2014**, *2*, 8069.
- (18) Luque, D.; de la Escosura, A.; Snijder, J.; Brasch, M.; Burnley, R. J.; Koay, M. S. T.; Carrascosa, J. L.; Wuite, G. J. L.; Roos, W. H.; Heck, A. J. R.; Cornelissen, J. J. L. M.; Torres, T.; Caston, J. R. *Chemical Science* **2014**, *5*, 575.
- (19) Brasch, M.; de la Escosura, A.; Ma, Y.; Uetrecht, C.; Heck, A. J. R.; Torres, T.; Cornelissen, J. J. L. M. *Journal of the American Chemical Society* **2011**, *133*, 6878.
- (20) Cheng, Y.; Zhao, L.; Li, Y.; Xu, T. *Chemical Society Reviews* **2011**, *40*, 2673.
- (21) Tian, W.-d.; Ma, Y.-q. *Chemical Society Reviews* **2013**, *42*, 705.
- (22) Zhu, J.; Shi, X. *Journal of Materials Chemistry B* **2013**, *1*, 4199.
- (23) Wolinsky, J. B.; Grinstaff, M. W. *Advanced Drug Delivery Reviews* **2008**, *60*, 1037.
- (24) Jiang, D.-L.; Aida, T. *Chemical Communications* **1996**, 1523.
- (25) Jang, W. D.; Nishiyama, N.; Zhang, G. D.; Harada, A.; Jiang, D. L.; Kawauchi, S.; Morimoto, Y.; Kikuchi, M.; Koyama, H.; Aida, T.; Kataoka, K. *Angewandte Chemie-International Edition* **2005**, *44*, 419.
- (26) Li, W.; Zhang, A.; Schluter, A. D. *Macromolecules* **2008**, *41*, 43.
- (27) Li, W.; Zhang, A.; Schluter, A. D. *Chemical Communications* **2008**, 5523.
- (28) Guo, Y. F.; Zhao, Y. N.; Zhao, J.; Han, M. H.; Zhang, A. F.; Wang, X. T. *Bioconjugate Chemistry* **2014**, *25*, 24.
- (29) Sun, H. L.; Guo, B. N.; Cheng, R.; Meng, F. H.; Liu, H. Y.; Zhong, Z. Y. *Biomaterials* **2009**, *30*, 6358.
- (30) Khorsand, B.; Lapointe, G.; Brett, C.; Oh, J. K. *Biomacromolecules* **2013**, *14*, 2103.
- (31) Chen, W.; Meng, F.; Li, F.; Ji, S.-J.; Zhong, Z. *Biomacromolecules* **2009**, *10*, 1727.
- (32) Meng, F.; Zhong, Z.; Feijen, J. *Biomacromolecules* **2009**, *10*, 197.
- (33) Rapoport, N. *Progress in Polymer Science* **2007**, *32*, 962.
- (34) Rodríguez-Hernández, J.; Chécot, F.; Gnanou, Y.; Lecommandoux, S. *Progress in Polymer Science* **2005**, *30*, 691.
- (35) Schmaljohann, D. *Advanced Drug Delivery Reviews* **2006**, *58*, 1655.
- (36) You, Y.-Z.; Hong, C.-Y.; Pan, C.-Y. *Macromolecules* **2009**, *42*, 573.
- (37) Savić, R.; Luo, L.; Eisenberg, A.; Maysinger, D. *Science* **2003**, *300*, 615.
- (38) Ding, J.; Chen, J.; Li, D.; Xiao, C.; Zhang, J.; He, C.; Zhuang, X.; Chen, X. *Journal of Materials Chemistry B* **2013**, *1*, 69.
- (39) Li, Z.-Y.; Hu, J.-J.; Xu, Q.; Chen, S.; Jia, H.-Z.; Sun, Y.-X.; Zhuo, R.-X.; Zhang, X.-Z. *Journal of Materials Chemistry B* **2015**, *3*, 39.
- (40) Yue, D.; Cheng, G.; He, Y.; Nie, Y.; Jiang, Q.; Cai, X.; Gu, Z. *Journal of Materials Chemistry B* **2014**, *2*, 7210.
- (41) Saito, G.; Swanson, J. A.; Lee, K.-D. *Advanced Drug Delivery Reviews* **2003**, *55*, 199.
- (42) Hwang, C.; Sinskey, A.; Lodish, H. *Science* **1992**, *257*, 1496.
- (43) Dong, W.-F.; Kishimura, A.; Anraku, Y.; Chuanoi, S.; Kataoka, K. *Journal of the American Chemical Society* **2009**, *131*, 3804.
- (44) Kim, J. O.; Sahay, G.; Kabanov, A. V.; Bronich, T. K. *Biomacromolecules* **2010**, *11*, 919.
- (45) Kim, S. H.; Jeong, J. H.; Lee, S. H.; Kim, S. W.; Park, T. G. *Journal of Controlled Release* **2006**, *116*, 123.
- (46) Read, E. S.; Armes, S. P. *Chemical Communications* **2007**, 3021.
- (47) Cheng, R.; Meng, F. H.; Ma, S. B.; Xu, H. F.; Liu, H. Y.; Jing, X. B.; Zhong, Z. Y. *Journal of Materials Chemistry* **2011**, *21*, 19013.
- (48) Meng, F. H.; Hennink, W. E.; Zhong, Z. *Biomaterials* **2009**, *30*, 2180.
- (49) Bolisetty, S.; Schneider, C.; Polzer, F.; Ballauff, M.; Li, W.; Zhang, A.; Schlüter, A. D. *Macromolecules* **2009**, *42*, 7122.
- (50) Nawaz, M. H.; Xu, L.; Liu, F.; Zhang, W. A. *Rsc Advances* **2013**, *3*, 9206.
- (51) Li, Z. Y.; Wang, H. Y.; Li, C.; Zhang, X. L.; Wu, X. J.; Qin, S. Y.; Zhang, X. Z.; Zhuo, R. X. *Journal of Polymer Science Part A - Polymer Chemistry* **2011**, *49*, 286.
- (52) Turner, G. K. *Science* **1964**, *146*, 183.
- (53) Brannon, J. H.; Magde, D. *Journal of the American Chemical Society* **1980**, *102*, 62.
- (54) Ng, A. C. H.; Li, X. Y.; Ng, D. K. P. *Macromolecules* **1999**, *32*, 5292.
- (55) SPILLER, W.; KLIESCH, H.; WÖHRLE, D.; HACKBARTH, S.; RÖDER, B.; SCHNURPFEIL, G. *Journal of Porphyrins and Phthalocyanines* **1998**, *02*, 145.

Journal Name

- (56) Zou, Y.; Brooks, D. E.; Kizhakkedathu, J. N. *Macromolecules* **2008**, *41*, 5393.
- (57) Karlstroem, G.; Carlsson, A.; Lindman, B. *The Journal of Physical Chemistry* **1990**, *94*, 5005.
- (58) Sahay, G.; Batrakova, E. V.; Kabanov, A. V. *Bioconjugate Chemistry* **2008**, *19*, 2023.
- (59) Yoo, H. S.; Lee, K. H.; Oh, J. E.; Park, T. G. *Journal of Controlled Release* **2000**, *68*, 419.